Inorganic Chemistry

Article

pubs.acs.org/IC

$Sr_{21}Bi_8Cu_2(CO_3)_2O_{41}$, a Bi^{5+} Oxycarbonate with an Original 10L Structure

Sylvie Malo,*[,†] Artem M. Abakumov,[§] Marco Daturi,[‡] Denis Pelloquin,[†] Gustaaf Van Tendeloo,[§] Anne Guesdon,[†] and Maryvonne Hervieu[†]

[†]Laboratoire CRISMAT and [‡]Laboratoire LCS, ENSICAEN-UCBN, 6 Bld Maréchal Juin, 14050 Caen, France

[§]EMAT, University of Antwerp, Groenenborgerlaan 171, B-2020 Antwerpen, Belgium

Supporting Information

ABSTRACT: The layered structure of $Sr_{21}Bi_8Cu_2(CO_3)_2O_{41}$ (Z = 2) was determined by transmission electron microscopy, infrared spectroscopy, and powder X-ray diffraction refinement in space group $P6_3/mcm$ (No. 194), with a = 10.0966(3)Å and c = 26.3762(5)Å. This original 10L-type structure is built from two structural blocks, namely, $[Sr_{15}Bi_6Cu_2(CO_3)O_{29}]$ and $[Sr_6Bi_2(CO_3)O_{12}]$. The Bi^{5+} cations form $[Bi_2O_{10}]$ dimers, whereas the Cu^{2+} and C atoms occupy infinite tunnels running along $\vec{c}$. The nature of the different blocks and layers is discussed with regard to the existing hexagonal layered compounds. $Sr_{21}Bi_8Cu_2(CO_3)_2O_{41}$ is insulating and paramagnetic.

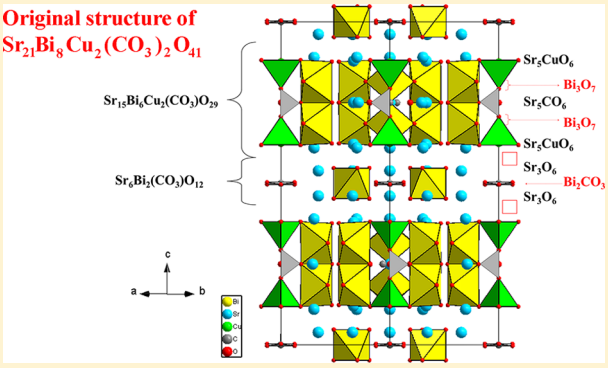

INTRODUCTION

The majority of metals form carbonated salts, an important class of materials in numerous industrial processes as well as in earth sciences. After the discovery of high T_c superconducting (HT_cS) properties in Bi-based cuprates[1−3] and the formation of carbonated layers in the perovskite-related $Sr_2CuCO_3O_2$,[4] numerous papers have been devoted to the studies of oxycarbonates enlarged to other M transition elements to form now a true family of materials. The richness of their chemistry is due to the ability of the CO_3 groups (or similar) to be easily introduced in oxide frameworks, creating then a large range of structural units, from local substitution in MO_x polyhedra to fully carbonated layers as in the mineral $Bi_2CO_3O_2$[5] and HT_cS relatives.[6] In the first perovskite-related compound $Sr_2CuCO_3O_2$,[4] the CO_3 groups adopt the so-called "flag" configuration and, in the Bi-based carbonates, the "coat hanger" configuration, keeping a unique direction in the bismutite or pointing up and down in beyerite and kettnerite.[5,7,8] In the strontionite form of $SrCO_3$, the CO_3 groups are roughly parallel to the layer plane but slightly nonplanar, the aplanarity being defined by the distance between the C atom and the plane formed by its three neighboring O atoms. Such a "flattened" arrangement of the carbonate groups is similar to that observed in $Ca_4Tl_2(CO_3)O_6$,[9] where they also form full carbonated layers.

Another interesting consequence of the carbonation mechanism deals with the fact that the creation of carbonated structural units involves potential property variations, by changes of the symmetry and cation oxidation states, and, also, carbonated structural units allow the synthesis of metastable phases as exemplified for materials deposited in the form of thin film.[10]

In the course to HT_cS Bi-based cuprates and their complex modulated structures,[2] the Bi−Sr−Cu−O system has been extensively studied.[3−5,10−12] A large part of the papers was devoted to the Cu-rich part of the diagram,[11] close to the $Bi_2Sr_2CuO_{6+\delta}$[3−6] composition. In the same way, the discovery of the possible substitution, in the perovskite blocks, of one octahedral $[MO_2]_\infty$ layer by one carbonate layer[13] generates superconducting Cu-based oxycarbonates,[10,14,15] has encouraged the exploration of oxycarbonates. This is the case of the $Sr_6Bi_2Cu_3(CO_3)_2O_{10}$.[16] For a close Sr/Bi ratio, two phases have been reported, namely, $Sr_6Bi_2^{3+}O_9$[17,18] and one ordered perovskite $Sr_6Bi_2^{5+}O_{11}$.[19] The studies carried out on the Bi-, Sr-, and Cu-based oxycarbonates have highlighted the ability of these perovskite-related frameworks to adapt CO_2^{3-} anions, but no oxycarbonate had been reported, up to our knowledge, in the Cu-poor zones of the Bi−Sr−Cu−O systems.

In this paper, we report on the exploration of this part of the diagram and show that a new layered compound, $Sr_{21}Bi_8Cu_2(CO_3)_2O_{41}$, is stabilized by the presence of CO_2^{3-} groups. This oxycarbonate was studied using X-ray powder diffraction (XRPD) data, infrared (IR) spectroscopy, and transmission electron microscopy (TEM) techniques.

Received: June 6, 2014
Published: September 17, 2014

 © 2014 American Chemical Society

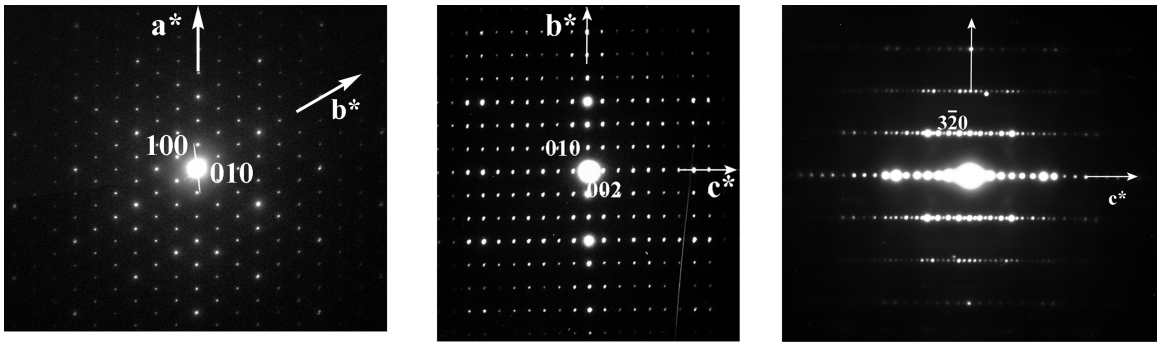

Figure 1. $Sr_{21}Bi_8Cu_2(CO_3)_2O_{41}$ (a) [001], (b) [110], and (c) [140] ED patterns.

EXPERIMENTAL SECTION

The samples were prepared by solid-state reaction, starting from Bi_2O_3, SrO_2−SrO−$SrCO_3$, and CuO. Once the new phase was detected, using PXRD and electron diffraction data, and its Bi/Sr/Cu ratio was determined by energy dispersive spectroscopy (EDS), the nominal oxygen and carbonate stoichiometry were adjusted from the $SrO/SrO_2/SrCO_3$ ratios and were varied to obtain single-phased samples. The title compound was prepared from mixtures of $4Bi_2O_3$, $SrCO_3$, 10SrO, $10SrO_2$, and 2CuO. SrO was calcined at 1200 °C and introduced, still burning, in a nitrogen-filled glovebox to be intimately ground with the other precursors and pressed in the form of bars. They were then introduced into alumina fingers and placed in quartz-sealed ampule under primary vacuum. The samples were heated from room temperature (RT) to 900 °C in 6 h, maintained at this temperature for 15 h, and then cooled to ambient temperatures in 6 h.

The phase identifications were carried out with a Panalytical Xpert Pro diffractometer, equipped with a graphite secondary monochromator and working with Cu Kα radiation. The XRPD data were collected by step scanning (0.02°) from 10° to 120°, by 2θ. Rietveld refinement of the XRPD data was performed using the program package JANA 2006.[20]

Samples for TEM were prepared by crushing the crystallites in ethanol, and the small flakes were deposited on a holey carbon film. The electron diffraction (ED) study was carried out using a JEOL 2010CX electron microscope (tilt = ± 60°) equipped with an EDS analyzer. The reciprocal space was reconstructed by tilting around the crystallographic axes. The high-resolution electron microscopy (HREM) images were recorded with a TOPCON 02B microscope (200 kV and spherical aberration constant = 0.4 mm) and a JEOL 4000 (400 kV and spherical aberration constant = 1 mm). High-angle annular dark-field scanning transmission electron microscopy (HAADF-STEM) images were recorded on a Tecnai G^2 microscope (200 kV).

For the IR spectroscopy study, the sample was pressed (~10^6 Torr) into self-supported disks (2 cm^2 area) and placed in a specifically designed holder. The wafers were obtained accurately by mixing and grinding 98 mg of KBr with 2 mg of the product powder to obtain the desired dilution, to decrease the intensity of the structural bands and prevent signal saturation. IR spectra (64 scans per spectrum) were collected using a Thermo Scientific Nicolet 6700 spectrometer, equipped with a DTGS detector and a KBr beam splitter. Spectra were recorded at room temperature in the range of 4000−400 cm^{-1}, at a resolution of 4 cm^{-1}, and 64 scans were accumulated for each spectrum.

Magnetic susceptibility was measured with an alternating current−direct current Squid Quantum Design Company magnetometer from Physical Properties Measurements System in the range of 5−400 K.

RESULTS

According the above synthesis conditions, a well-crystallized and black single-phased sample is obtained.

Electron Diffraction of $Sr_{21}Bi_8Cu_2(CO_3)_2O_{41}$. The reconstruction of the reciprocal space showed that the compound crystallizes in a hexagonal cell, with $a \approx 10$ Å and $c = 26.4$ Å. Typical ED patterns are given in Figure 1. The [001] (Figure 1a) and [140] (Figure 1c) ED patterns evidence the absence of limiting condition for the *hkil* reflections whereas the condition $h\bar{h}0l$, $l = 2n$ (Figure 1b), is consistent with the $P6_3/mcm$ space group. The EDS analyses carried out on numerous crystallites confirmed the actual average cationic ratio Sr/Bi/Cu close to 10.6(2)/3.9(2)/1.3(2), in agreement with the nominal composition.

Infrared Analysis. The spectrum of the compound collected after dilution in KBr (Figure 2a) presents a broad feature at 3440 cm^{-1} due to adsorbed water on the highly

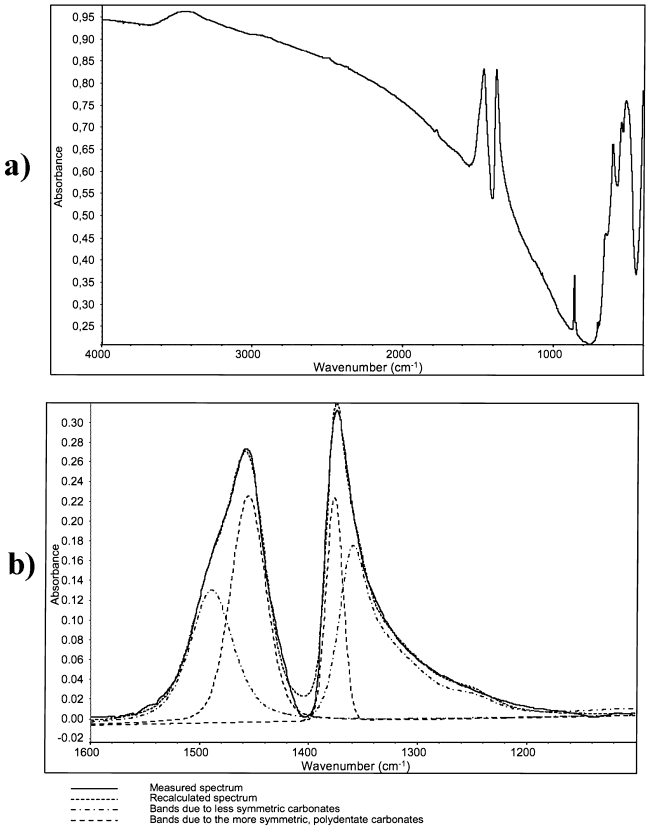

Figure 2. (a) IR spectrum registered at room temperature. (b) Deconvolution of the carbonate massif for quantifying the two species.

dx.doi.org/10.1021/ic501322w | Inorg. Chem. 2014, 53, 10266−10275

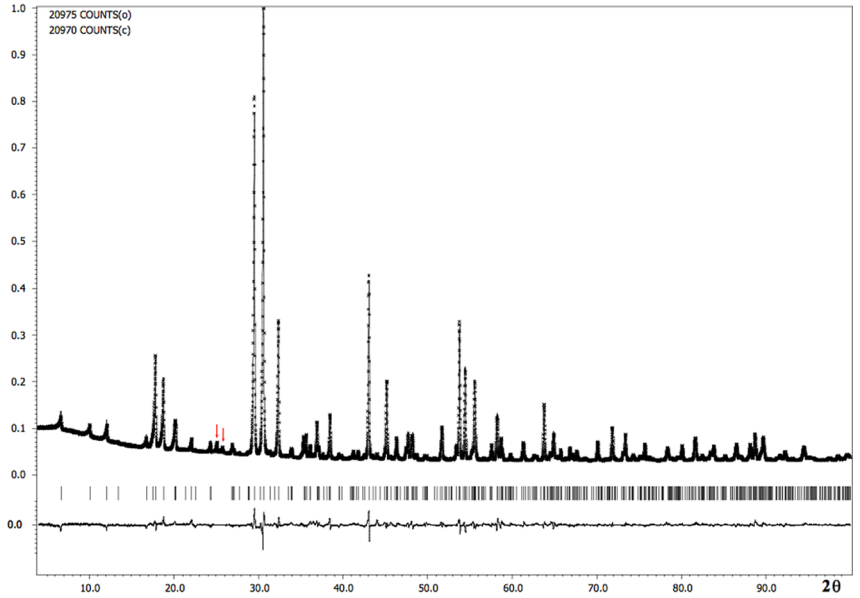

Figure 3. XRPD pattern of $Sr_{21}Bi_8Cu_2(CO_3)_2O_{41}$ (Z = 2) indexed in the $P6_3/mcm$ (vertical bars) in which the red arrows indicate two peaks associated with a nonidentified impurity. Reliability factors: R_p (obs) = 0.0287; R_{wp} (obs) = 0.0397; GOF = 1.34; R(obs) = 0.0395; R_w (obs) = 0.0304.

hygroscopic potassium bromide (water vapor adsorbed from air during the experimental manipulation). Two main bands can be observed at 1458 and 1374 cm^{-1}, in the region of the ν(OCO) stretches.[21] At lower wavenumbers, bands due to the skeletal vibrations of cations and oxygen atoms are detected. Below, only the features assigned to carbonates will be discussed.

To better scrutinize the spectrum, a zoom was made in the 1600−1100 cm^{-1} region. It appeared that the two main bands constitute a more complex massif containing at least 4 peaks, at 1489, 1455, 1376, and 1360 cm^{-1}, the latter having a long tail extended over about 100 cm^{-1}. The minimum of the massif is centered near 1415 cm^{-1}, close to the position of the ν_3 double degenerate band of the free carbonate ion having a D_{3h} symmetry.[21] Therefore, the four maxima observed in the spectrum should be interpreted as two pairs of bands resulting from the split of the degenerate ν_3 vibration after symmetry (partial) lost.[21] As a consequence, two carbonate species should be considered, the first characterized by the bands at 1489 and 1360 cm^{-1}, the second associated with the doublet at 1455 and 1376 cm^{-1}. Both moieties are ionic carbonates, the $\Delta\nu_3$ splitting being less than 150 cm^{-1}.[22] Obviously, the smaller the $\Delta\nu_3$ splitting, the more symmetric the structure, therefore we could assign the species associated with the 1455 and 1376 cm^{-1} bands to the polydentate carbonates in the aragonite blocks.[22] Conversely, the more distorted species (components at 1489 and 1360 cm^{-1}, associated with a broad tail as well, witnessing for a distortion or a high degree of freedom in the structure) present a configuration coherent with the flag configuration of the carbonate group.

A tentative quantification of the aforementioned species has been performed by deconvoluting the carbonate massif (see Figure 2b): the relative integrated area of the corresponding peaks for the two species give an approximate relative value of 0.79 for the more symmetric respect to the more distorted species. Considering the overestimation induced by the low wavenumber tail, the amount of carbonates in both crystallographic sites can be considered as equivalent.

Structural Determination. The XRPD pattern is given in Figure 3. The cell parameters were refined to a = 10.0966(3)Å and c = 26.3762(5) Å, for a cell volume of 230.6 $Å^3$, assuming the $P6_3/mcm$ space group. The XRPD pattern of the present sample is close to the one recorded by Saggio et al., obtained in the course investigation of the Bi/Sr/Cu/O system, using Li_2CO_3 as mineralizer.[12] However, as the reported parameters and symmetry of the structures are different, the structural analysis was carried out (R_p = 0.0287; R_{wp} = 0.0397; GOF = 1.34).

The layer stacking mode of the different layers was solved by combined XRPD data, TEM studies, and taking into account the inset of carbonate groups confirmed by the results of IR. After a Lebail profile analysis, the diffraction peak intensities were extracted and treated with the charge-flipping algorithm (SuperFlip routine) implemented in JANA software.[20] In this way, a consistent cation framework could be found. A part of the carbonate group positions can be deduced from Fourier analyses. As shown on the Fourier difference map calculated at z = 0 (Figure 4), a distinct electron density peak surrounded by six equivalent smaller peaks (red marks) can be observed in the central position. The latter electron residues are 1.3−1.4 Å from the central peak and can be associated with the O8 oxygen position randomly arranged around the carbon C1 (see Table 1). A second set of carbonate group related to the carbon C2 position (Table 1) can be highlighted from high-resolution observations.

The HREM study was carried out using both HREM and HAADF-STEM techniques. The combination of them allows determining the structural characteristics of the new structure. Examples of [100] and [110] HREM images are given in Figure 5a,b; the simulated images calculated for the refined positional parameters given in Table 1 (focus −650 Å and −100 Å for Figure 5a,b, respectively, and thickness close to 35 Å) are superposed to the experimental ones. Along the [100] viewing direction, the Bi and Sr atoms appear as the brighter dots in Figure 5a in two different blocks (blue and red). The double brighter dots of the Bi dimers are marked by a red oval on both

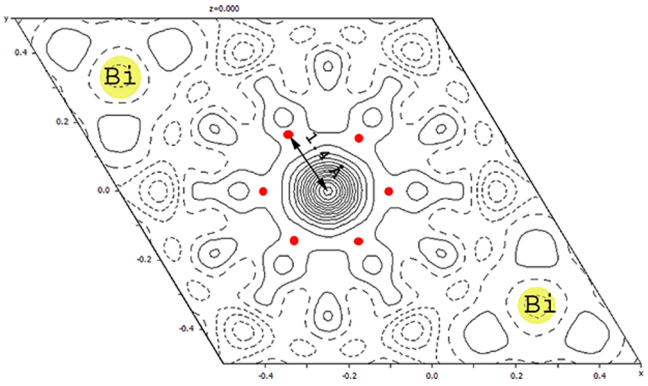

Figure 4. Fourier difference map evidencing the flat configuration of the carbonate group at $z = 0$ (for establishing the map, the calculated density was performed with the atomic structure detailed in Table 1 without the C1 and O8 positions pointed by the black and red arrows, respectively).

the experimental image and the projected atomic positions (Sr in blue and Bi in yellow). Along the [110] viewing direction, in Figure 5b, the high electron density zones appear as the darker ones, and the two structural blocks [AA′A]-type $[Sr_{15}Bi_6Cu_2(CO_3)O_{29}]$ and hh-type $[Sr_6Bi_2(CO_3)O_{12}]$ are also clearly differentiated: the small bright crosses are associated with the presence of the carbonate groups of the h-type block (see the blue arrow in the inserted simulated image) (C1 position in Table 1), whereas the vertical line of brighter dots, parallel to the *c* axis (see vertical green arrow), are associated with the zone of lighter electron density, in between the Sr and Bi atoms of the [AA′A]-type block, and related to the second set of carbonate (C2 position in Table 1).

The HAADF-STEM images provide a "map" of the distribution of the "higher Z" cations in the crystal. The two structural blocks are also clearly identified in the [110] HAADF images, with the darker zone associated with the low electron density zone, associated with the carbonate positions of the *hh*-type block, as observed in Figure 6a; the projected positions of the Bi cations are superposed to the enlargement (left). Along the [001] direction (Figure 6b), the contrast is more complex because Bi and Sr are projected over almost the same positions along $\vec{c}$. The contrast consists in the alternation of two lines of brighter zones (yellow arrows) and one less light (red arrow) along the equivalent directions of the hexagonal cell. The brighter ones are associated with the projection of the columns of Bi and Sr atoms, as observed with the superposition of the projected positions of Sr (blue circles) and Bi/Sr (yellow on blue); the small red arrows indicate the darker zone associated with the superposition of the Cu and C positions along $\vec{c}$. Between the up and down parts of the image, a shifting of the structure (follow the yellow arrows parallel to the ***a*** axis) is observed; this phenomenon is discussed in a next section.

Description of the 10L Structure. The refinements of the atomic parameters, leading to the formulation $Sr_{21}Bi_8Cu_2(CO_3)_2O_{41}$ ($Z = 2$), are consistent with the EDS results and the oxidizing conditions of the synthesis process, suggesting a pentavalence of the bismuth atoms. The structural model according to a 10L structure, established from the refinement of the XRD data accounting the TEM observations, is drawn in Figure 7a; the composition of each of the layers stacked along ***c*** is indicated. The refined positional parameters are given in Table 1, and the interatomic distances calculated from these positions are given in Table 2. Additional crystallographic data are available in the Supporting Information.

Three different strontium layers are observed, namely, $[Sr_5CuO_6]$, $[Sr_5(CO_3)O_3]$, and $[Sr_3O_6]$, sandwiching two types of bismuth layers, namely, $[Bi_3O_7]$ and $[Bi_2(CO_3)]$, where Bi^{5+} cations adopt an octahedral coordination; one octahedral layer is empty, marked □ in Figure 7a. The structure can be described as built up from two blocks, having the same *a* and *b* parameters but different *c* parameters, separated by a layer of empty octahedra. The two intergrown structural blocks in which the strontium layers adopt different stacking mode: [AA′A] in the $[Sr_{15}Bi_6Cu_2(CO_3)O_{29}]$ and *hh* in the $[Sr_6Bi_2(CO_3)O_{12}]$ block.

Within the [AA′A]-type block, $[Sr_{15}Bi_6Cu_2(CO_3)O_{29}]$, the pentavalent bismuth atoms located in the $[Bi_3O_7]$ layers form

Table 1. Structural Parameters of $Sr_{21}Bi_8Cu_2(CO_3)_2O_{41}$[a]

atom	occupancy	*x*	*y*	*z*	U_{iso} (Å^2)
Bi1	1	0.66766(15)	0	0.18315(6)	0.0011(2)
Bi2	1	0.6667	0.3333	0	0.0011(2)
Sr1	1	0.2902(4)	0	0.25	0.007(2)
Sr2	1	0.6567(4)	0	0.03882(13)	0.017(1)
Sr3	1	0.6667	0.3333	0.12101(13)	0.003
Sr4	1	0	0.3040(3)	0.11008(10)	0.003(1)
Sr5	1	0.3333	0.6667	0.25	0.029(2)
Cu1	1	0	0	0.1280(4)	0.007(2)
C1	1	0	0	0	0.027(2)
C2	0.3333	0.0642(10)	0.0642(10)	0.25	0.027(2)
O1	1	0.5139(11)	0.7017(13)	0.0473(5)	0.016(2)
O2	1	0.1801(19)	0.1801(19)	0.1188(8)	0.016(2)
O3	1	0.5708(13)	0.7762(11)	0.1850(5)	0.016(2)
O4	1	0.468(3)	0.468(3)	0.25	0.016(2)
O5	1	0.467(2)	0.467(2)	0.1236(7)	0.016(2)
O6	1	0	0.814(2)	0.25	0.016(2)
O7	1	0	0	0.207	0.016(2)
O8	0.5	0.1265(6)	0	−0.0032(18)	0.016(2)

[a] $Z = 2$; space group = $P6_3/mcm$.

dx.doi.org/10.1021/ic501322w | *Inorg. Chem.* 2014, 53, 10266−10275

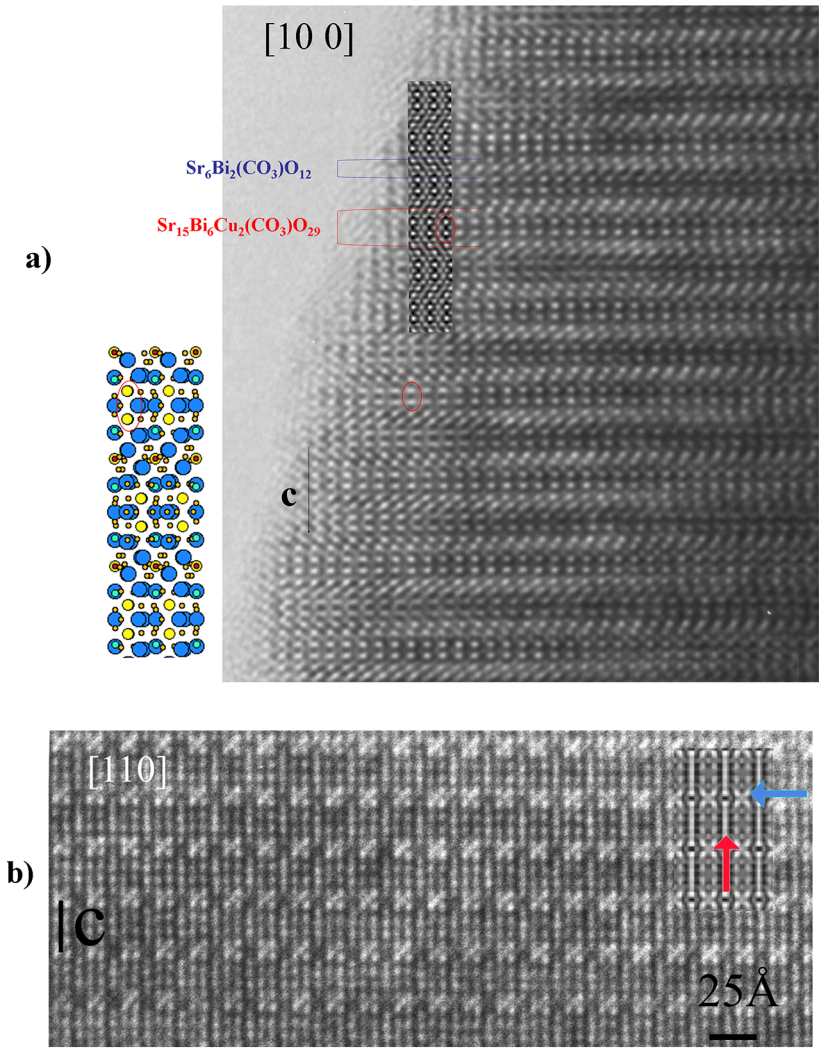

Figure 5. HREM images of $Sr_{21}Bi_8Cu_2(CO_3)_2O_{41}$. (a) [100] and (b) [110]. The corresponding structural model is drawn, and both carbonate groups are pointed out in blue and red, respectively.

Bi_2O_{10} dimers, built up from edge-sharing distorted octahedra. At the level of the A layers, one Sr is replaced by one Cu atom in tetrahedron (represented in green), whereas at the level of the A′ intermediate Sr layer, one Sr is replaced by the C of one carbonate group in flag configuration. The Bi_2O_{10} dimers, with the interatomic distances, are drawn in Figure 7b. Similar Bi_2O_{10} dimers have been observed in the trirutile structure of $MgBi_2O_6$[23] and $LiBiO_3$.[24] Within the *hh*-type block, $[Sr_6Bi_2(CO_3)O_{12}]$, the Bi^{5+} atoms occupy regular isolated octahedra (with d_{Bi-O} = 2.09 Å). In this block, the carbonate groups are roughly parallel to the hexagonal plane. The two configurations observed for the carbonate groups, that is, in-plane in the $Sr_6Bi_2(CO_3)O_{12}$ block and flag configurations in the $Sr_{15}Bi_6Cu_2(CO_3)O_{29}$ block, are consistent with the IR spectroscopy analysis results. The Sr atoms exhibit two types of coordination polyhedra: the coordination is VII or IX as they have one neighbor Cu or CO_3 group, in the $[Sr_5CuO_6]$ and $[Sr_5CO_6]$ layers and VII with six Sr neighbors, in the $[Sr_3O_6]$ layers.

Linear Defects. The HAADF-STEM images, together with the HREM observations, evidence the regular distribution of the different types of atoms, the heavier Bi and Sr, on the one hand, and the lighter ones, Cu, C, and O, on the other hand. They also show the high regularity of the stacking mode of the blocks and different layers in the structure; only tiny local variations of the contrast were observed.

Deviations from this regular structure are sometimes detected in the form of linear defects; they are associated with local variations of contrast at the level of the positions of the carbonate groups located in the *hh*-type block. One example of [110] HREM image is given in Figure 8a where the defective zone appears as diffuse darker lines, forming geometrical domains.

These boundaries (see black arrows) run along $[1\bar{1}0]$, $[1\bar{1}2]$, $[\bar{1}12]$, and equivalents. Two parts of the image are enlarged, showing two directions of the domain boundaries (D.B.). The $[1\bar{1}0]$ boundary (dotted blue rectangle) is enlarged at the bottom part of the figure, and the two others are shown in the left part (dotted green rectangle). In this image, the brighter zones are associated with the light electron density zones and the horizontal brighter line to the $[Bi_2(CO_3)]$ layer of the "*hh*" block. The contrast translation along that direction is one bright dot alternating with two less bright ones; this periodicity can be followed through the yellow arrows, which highlight the brighter dots associated with the empty space between two Bi atoms.

The position of carbonate groups is correlated to the gray zone in between the two less bright dots (indicated by the

dx.doi.org/10.1021/ic501322w | *Inorg. Chem.* 2014, 53, 10266−10275

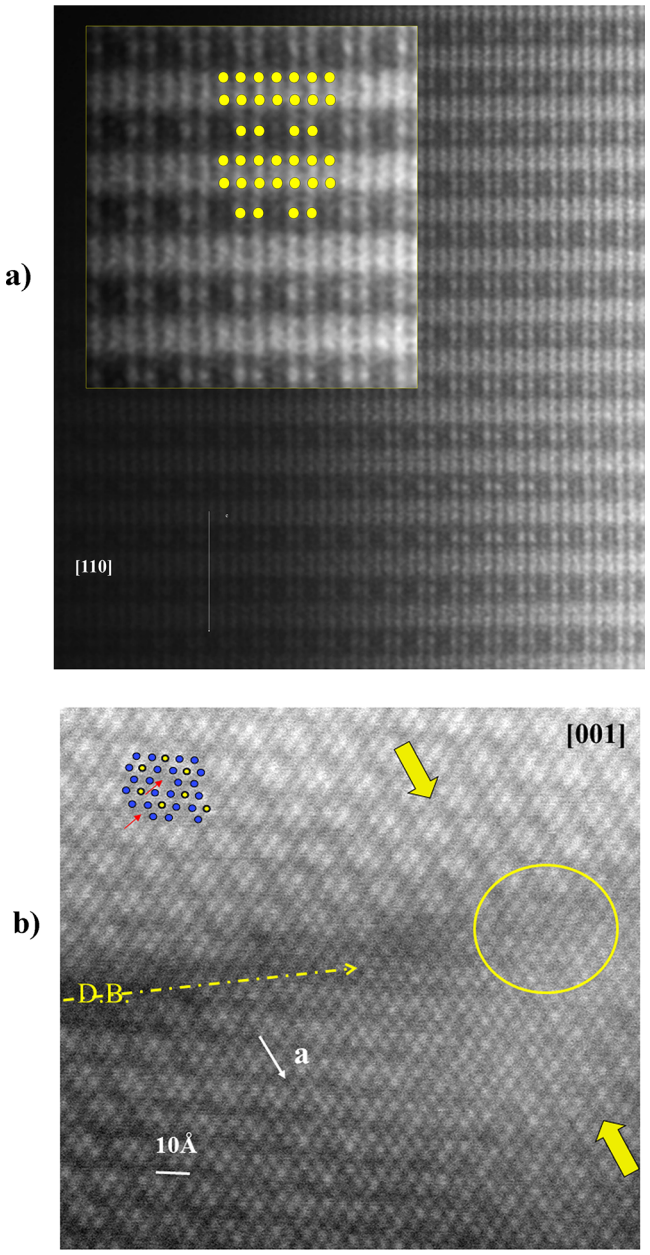

Figure 6. HAADF-STEM images. (a) [110]: the projected positions of the heavier Bi cations are superposed to the enlargement (yellow circles). (b) [001]: projection of the columns of Sr atoms (blue circles), Bi/Sr (yellow on blue), and the positions of the Cu,C indicated by red arrows. The relative shifting of the up and down parts of the image, indicated by yellow arrows, is related to linear defects detailed in Figure 8

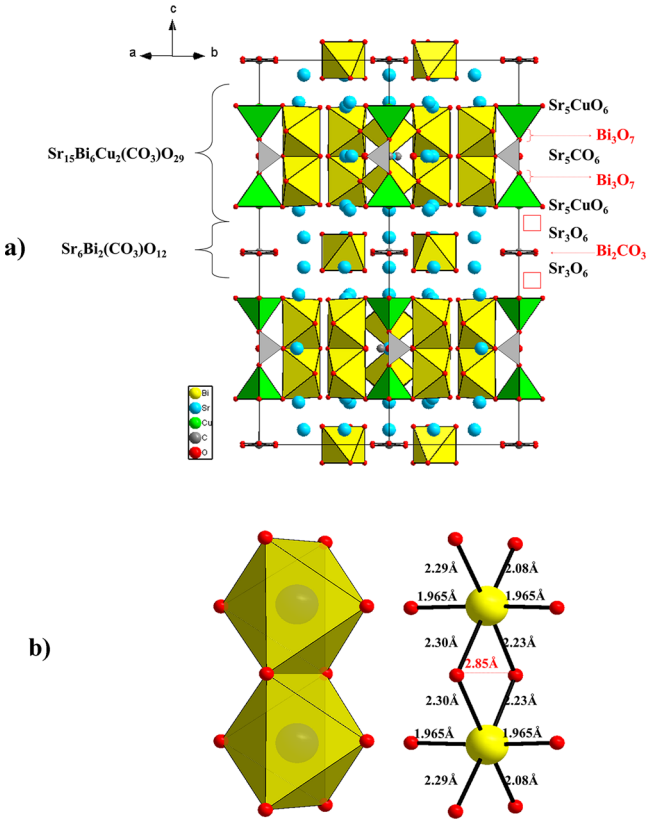

Figure 7. (a) Projection along [100] of the structural model of $Sr_{21}Bi_8Cu_2(CO_3)_2O_{41}$ and (b) Bi_2O_{10} dimer with the interatomic distances.

white long arrows). At the level of the defects, that is, of the domain boundaries, this sequence is no more observed (see red oval) but replaced by a sequence [one bright−one less bright] only. On this basis, a model was drawn (Figure 8b) on the hypothesis that these contrast variations suggest that one $[1\bar{1}0]$ slice $[Sr_5Bi_3O_3]$, one octahedron wide, is absent. The defects follow the $[1\bar{1}2]$ and $[\bar{1}12]$; the translation that the regular domains suffer on both sides of the D.B. is outlined by the vertical pink arrows. Such a translation induces a rupture of the columns of Cu and C atoms along *c*. As a consequence, by viewing thin crystallites along [001], the domain translation is also observed, and at the level of the boundaries, all the cations (Bi, Sr, Cu and C) are locally superposed. This is the aforementioned translation of the HAADF image (Figure 6b). The local rupture of the Cu and C columns results in the contrast disappearance between the different atom columns: this is clearly observed in the circled zone at the level of the D.B. with a uniform contrast.

Electrical and Magnetic Behavior. The electric resistivity of the $Sr_{21}Bi_8Cu_2(CO_3)_2O_{41}$ sample cannot be measured, due to the too-large resistivity, above the experimental limit at room temperature ($R > 10^6$ Ω).

The $\mathbf{M}(T)$ curve was recorded under a magnetic field of 0.3T. Figure 9 presents a curve characteristic of a paramagnetic behavior, consistent with a divalent copper compound, in agreement with the oxygen content O_{41}. (inset) The $\mathbf{M}(H)$ curve is also characteristic of a paramagnet. From the Curie−Weiss analysis of $\mathbf{M}(T)$ at high temperature, an effective moment of 2.10 μ_B/Cu was obtained, consistent with the 1.73 μ_B theoretically expected for an $S = 1/2$ system. The Curie−Weiss temperature is equal to −28 K.

Discussion and Concluding Remarks. In oxides, numerous 10L-type layered structures have been reported, as for example in the barium-based compounds $BaMnO_{3-x}$,[25] $Ba_{10}Ta_7Ti_{1.2}O_{30}$,[26] $Ba_5Ir_3CuO_{12}$,[27] $Ba_5In_2Al_2ZrO_{12}$,[28] or $Ba_5Ru_{1.6}W_{0.4}ZrCl_2O_9$.[29] The ratios between the cations (A/B and B atoms) and anions (X = O or Cl atoms) illustrate the possibilities offered by various mixed sequences of AX_3, AX_2, and AX layers, which manage octahedral or prismatic sites for the B cations. The nature of the Sr layers in the $Sr_{21}Bi_8Cu_2(CO_3)_2O_{41}$ structure is more complex, with two $[Sr_3O_6]$ (AX_2) and three AX-type layers; in two of them

dx.doi.org/10.1021/ic501322w | *Inorg. Chem.* 2014, 53, 10266−10275

Table 2. Selected Interatomic Distances in $Sr_{21}Bi_8Cu_2(CO_3)_2O_{41}$

atom1	atom 2	count	distance[a] (Å)
Bi1	O2	1×	2.29(2)
	O3	2×	1.965(9)
	O4	1×	2.23(2)
	O5	1×	2.08(2)
	O6	1×	2.30(2)
Bi2	O1	6×	2.088 (15)
Sr1	O3	4×	2.507(13)
	O4	1×	2.44(4)
	O6	2×	2.57(2)
Sr2	O1	2×	2.616(9)
	O1	2×	2.846(14)
	O2	1×	2.68(2)
	O5	1×	2.56(2)
	O8	1×	2.38(2)
Sr3	O1	3×	2.566(14)
	O3	3×	2.679(15)
	O5	3×	2.93(2)
Sr4	O1	2×	2.497(14)
	O2	2×	2.68(2)
	O3	2×	2.677(13)
	O5	1×	2.34(2)
Sr5	O3	6×	2.696(14)
	O4	3×	2.93(4)
C1	O8	3×	1.280(7)
C2	O6	1×	1.232(16)
	O7	2×	1.305(4)
Cu1	O2	3×	1.83(2)
	O7	1×	2.084(11)

[a]Reliability factors: R_p = 0.0287; R_{wp} = 0.0397; GOF = 1.34; R(obs) = 0.0395; R_w (obs) = 0.0304.

([Sr_5CuO_6]), Cu substitutes Sr, whereas, in the third one ([Sr_5CO_6]), the substituting carbonate group involves a distorted layer.

Besides the layered character of the present structure and the formation of two blocks, [AA′A] and *hh*, another original structural character of $Sr_{21}Bi_8Cu_2(CO_3)_2O_{41}$ deserves to be highlighted, that is, the formation of tunnels running along *c* where Cu atoms and carbonate groups alternate, as observed in the projection of the structure along [001] in Figure 10a. This architecture is clearly observed in the [110] HREM (Figure 5b) and [001] HAADF (Figure 5b) images. As shown viewing the structure along [001] (Figures 10a and 11a) and [110] (Figure 11b), they are bordered by the Bi and Sr polyhedra and only filled by Cu and C atoms

Hexagonal layered structures of oxides are often described as being derived of a hexagonal close packed or pseudo close packed of AX_2 and AX layers, as discussed in ref 30. As examples, in the 10L structures,[29,31,32] the ABA stacking mode of three Ba or Sr layers is adopted to form dimers, that is, the intermediate layer is always *h*-type. This is the case of the 10L-oxychloride $Ba_5Ru_{1.6}W_{0.4}Cl_2O_9$[29] (*h′hhhh′*), in which $(RuW)_2O_9$ dimers (Figure 12c) are formed between three BaO_3 layers in the sequence ABA (*hhh*). In the [$Sr_{15}Bi_6Cu_2(CO_3)O_{29}$] block of the title compound (Figure 12b), the sequence evidences the existence of pairs of adjacent layers of A type, [AA′A], so that the close packing arrangement of Sr layers is lost in the corresponding block, the Bi atoms keeping an octahedral environment with the formation of the

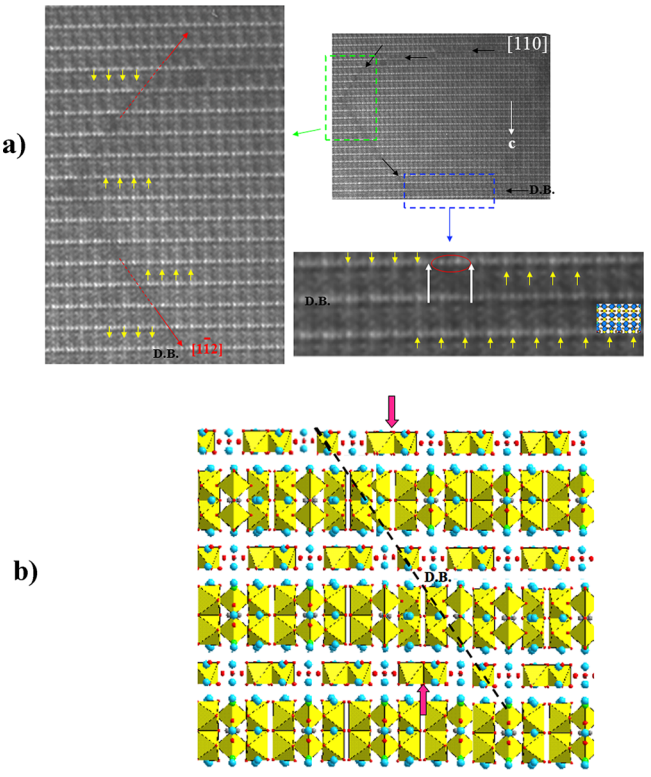

Figure 8. (a) [110] HREM image of a defective zone (the brighter zones are associated with the light electron density zones) and the two types of domain boundaries (D.B.) enlarged in the two dotted rectangles); (b) representation of the defect.

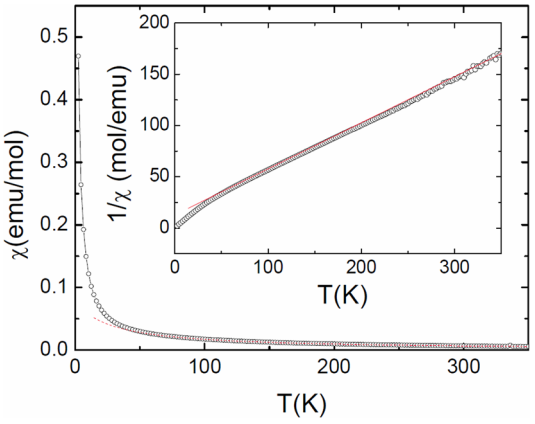

Figure 9. χ vs T and in insert 1/**M** vs **H** curves (2188.8 g·mol^{-1}).

dimer Bi_2O_{10} (instead of B_2O_9). A stacking mode close to the one observed in the title compound is observed in $Ca_{5-x}Ir_3O_{12}$,[33] [AA′A], where the IrO_6 octahedra sharing edge form infinite chains (Figure 12d) instead of dimers as in the present oxycarbonate. The [001] projection of the [$Sr_{15}Bi_6Cu_2(CO_3)O_{29}$] block (Figure 10c) shows that the dimers Bi_2O_{10} are isolated as the chains in $Ca_{5-x}Ir_3O_{12}$[33] (Figure 10d), the carbonate groups being located in the intermediate Sr layer (empty site in the iridate). The introduction of carbonate groups at the level of dimers in the hexagonal layered structures has been reported in the 6H-type oxycarbonate $Ba_3Ru_{1.74}(CO_3)_{0.31}Na_{0.95}O_{7.68}$.[34] In this compound, it was found that the C replaces one Ru atom located

dx.doi.org/10.1021/ic501322w | Inorg. Chem. 2014, 53, 10266−10275

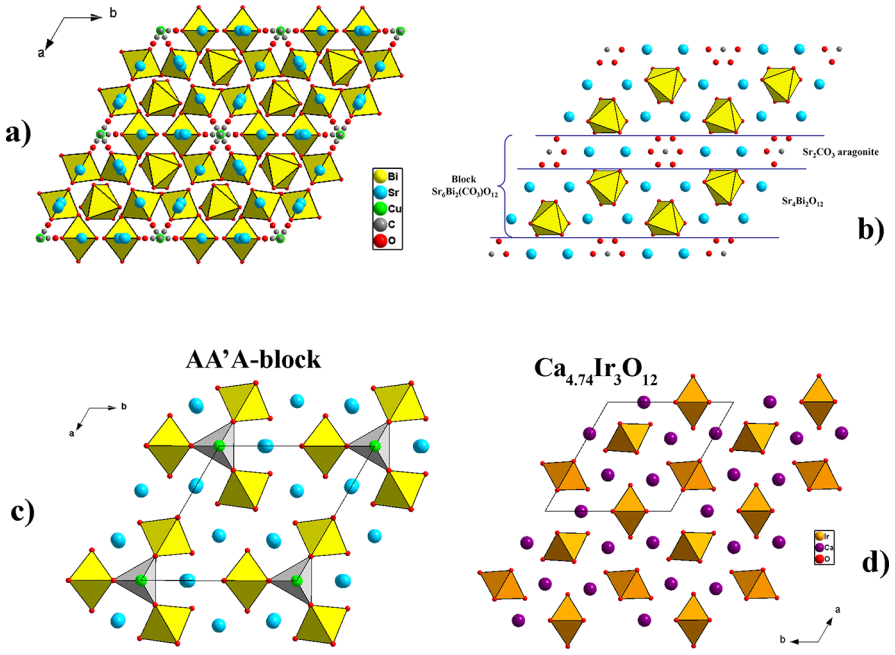

Figure 10. [001] projections showing (a) the Bi octahedra and tunnels in $Sr_{21}Bi_8Cu_2(CO_3)_2O_{41}$; (b) the aragonite-type slices in the $[Sr_6Bi_2(CO_3)O_{12}]$ blocks, and (c) comparison of the AA′A block in $Sr_{21}Bi_8Cu_2(CO_3)_2O_{41}$ with one slab of $Ca_{4.74}Ir_3O_{12}$.

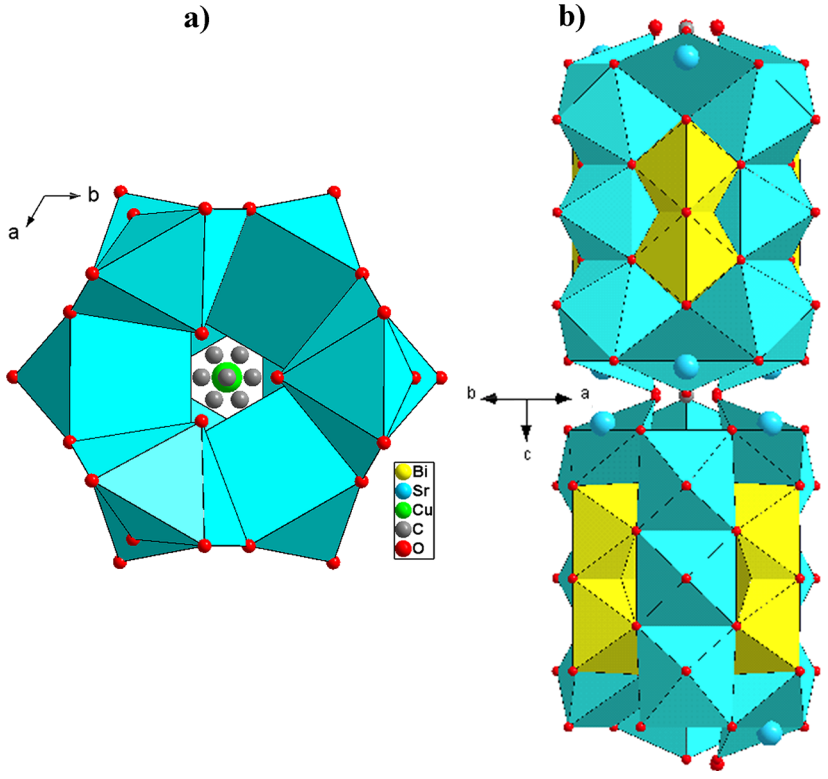

Figure 11. (a) [001] and (b) [110] views of the tunnels running along $\vec{c}$.

in the dimer Ru_2O_9 built up from to face-sharing octahedra in a *chcch* sequence.

In the *hh* block, one $[Bi_2(CO_3)]$ layer is sandwiched between two $[Sr_3O_6]$ layers. The [001] projected drawing (Figure 10a) shows that this block can also be described through parallel $[Sr_2CO_3]$ and $[Sr_4Bi_2O_{12}]$ slices (Figure 10b), similar to those observed in aragonite and previously described by Boulahya[35] in the 2H-type $Ba_3Co_2(CO_3)_{0.66}O_6$. The flattened arrangement of the carbonate groups is similar to the one observed in $Ca_4Tl_2(CO_3)O_6$,[9] where they form fully carbonated layers.

In conclusion, a new oxycarbonate $Sr_{21}Bi_8Cu_2(CO_3)_2O_{41}$ has been synthesized by controlling the ratio Sr/Bi/Cu and the introduction of carbonate groups; the latter ones adopt two configurations within each of the two building structural blocks $[Sr_{15}Bi_6Cu_2(CO_3)O_{29}]$ and $[Sr_6Bi_2(CO_3)O_{12}]$. The original 10L structure has been determined by TEM and XRPD

dx.doi.org/10.1021/ic501322w | *Inorg. Chem.* 2014, 53, 10266−10275

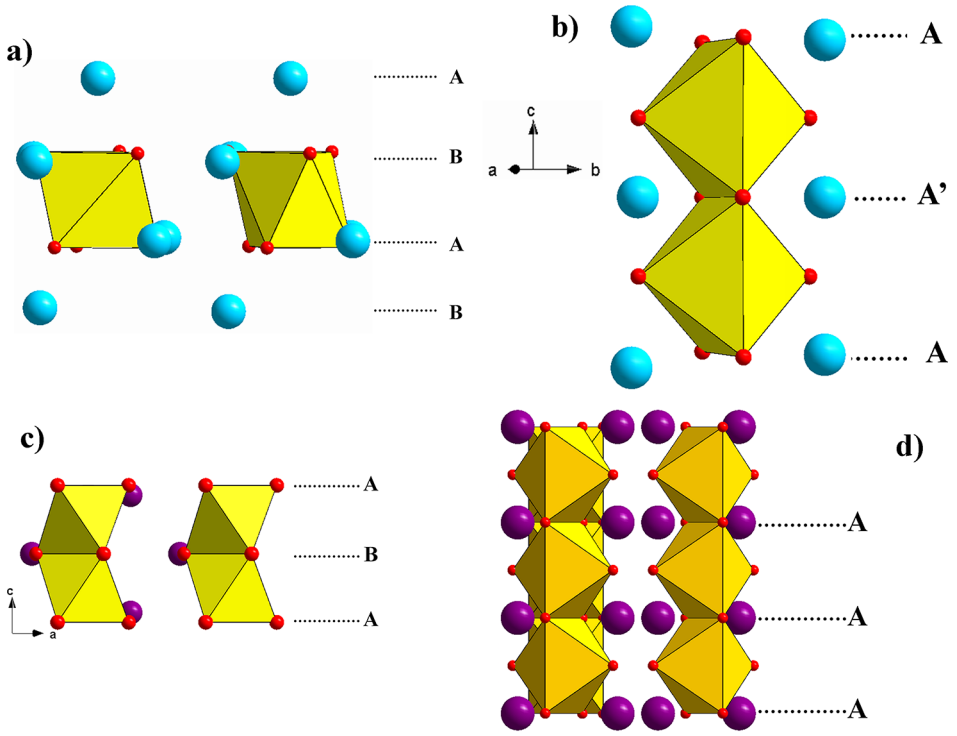

Figure 12. The stacking mode of the Sr layers in $Sr_{21}Bi_8Cu_2(CO_3)_2O_{41}$ (a) in the *hh* block and (b) AA′A between the dimers is compared to that of (c) $Ba_5Ru_{1.6}W_{0.4}Cl_2O_9$ and (d) $Ca_5Ir_3O_{12}$.

refinement, whereas the IR spectroscopic study has confirmed both the presence and configurations of carbonate groups in the framework. $Sr_{21}Bi_8Cu_2(CO_3)_2O_{41}$ is an insulating paramagnet.

■ ASSOCIATED CONTENT

Supporting Information

Structural and crystallographic information in the form of a CIF file. This material is available free of charge via the Internet at http://pubs.acs.org.

■ AUTHOR INFORMATION

Corresponding Author

*Corresponding author: sylvie.malo@ensicaen.fr.

Author Contributions

M.D., D.P., and M.H. contributed equally. The manuscript was written through contributions of all authors. All authors have given approval to the final version of the manuscript.

Notes

The authors declare no competing financial interest.

■ ACKNOWLEDGMENTS

The authors acknowledge Dr. S. Hébert (CRISMAT) for physical properties and Dr. C. Michel for X-ray analysis. Prof. S. Malo acknowledges ESTEEM network (ANT 200903300916) for financial support.

■ REFERENCES

(1) Michel, C.; Hervieu, M.; Borel, M. M.; Grandin, A.; Deslandes, F.; Provost, J.; Raveau, B. *Z. Phys. B: Condens. Matter* **1987**, *68*, 421.
(2) Raveau, B.; Michel, C.; Hervieu, M.; Groult, D. *Crystal Chemistry of High Tc Superconducting Copper Oxides;* Springer Series in Materials Science; Springer-Verlag: New York, 1991; Vol. *15*.
(3) Ikeda, Y.; Ito, H.; Shimomura, S.; Oue, Y.; Inaba, K.; Takano, M. *Phys. C* **1989**, *159*, 1−2.
(4) Miyazaki, Y.; Yamane, H.; Kajitani, T.; Oku, T.; Hiraga, K.; Morii, Y.; Fuchizaki, K.; Funahashi, S.; Hirai, T. *Phys. C* **1992**, *191*, 434.
(5) Grice, J. D. *Can. Mineral.* **2002**, *40*, 693.
(6) García-Alvarado, F.; Morán, E.; Alario-Franco, M. A.; González, M. A.; Vicent, J. L.; Cheetham, A. K.; Chippindale, A. M. *J. Less-Common Met.* **1990**, 164−165.
(7) Grice, J. D. *Can. Mineral.* **1999**, *37*, 923.
(8) Antao, S. M.; Hassan, I. *Can. Mineral.* **2009**, *47*, 1245.
(9) Caignaert, V.; Hervieu, M.; Goutenoire, F.; Raveau, B. *J. Solid State Chem.* **1995**, *116*, 321.
(10) Allen, J. L.; Mercey, B.; Prellier, W.; Hamet, J. F.; Hervieu, M.; Raveau, B. *Phys. C* **1995**, *241*, 158.
(11) Slobodin, B. V.; Ostapenko, I. A.; Fotiev, A. A. *Inorg. Mater.* **1991**, *27*, 2220.
(12) Saggio, J. A.; Sujata, K.; Hahn, J.; Hwu, S. J.; Poeppelmeier, K. R.; Mason, T. O. *J. Am. Ceram. Soc.* **1989**, *72*, 849.
(13) Greaves, C.; Slater, P. R. *Phys. C* **1991**, *175*, 172.
(14) Kinoshita, K.; Yamada, T. *Nature* **1992**, *357*, 313.
(15) Boullay, Ph.; Domenges, B.; Hervieu, M.; Raveau, B. *Chem. Mater.* **1993**, *5*, 1683.
(16) Pelloquin, D.; Maignan, A.; Caldes, M. T.; Hervieu, M.; Michel, C.; Raveau, B. *Phys. C* **1993**, *212*, 199.
(17) Roth, R.; Rawn, C.; Burton, B.; Beech, F. *J. Res. Natl. Inst. Stand. Technol.* **1990**, *95*, 291.
(18) Yang, Y.; Zhang, G.; Yu, S.; Shen, X. *Chem. Eng. J.* **2010**, *162*, 171.
(19) Bokhimi, X.; Portilla, M. *J. Solid State Chem.* **1993**, *105*, 371.
(20) Petříček, V.; Dušek, M.; Palatinus, L. *JANA2006;* Institute of Physics: Praha, Czech Republic, 2006.
(21) Nakamoto, K. *Infrared and Raman Spectra of Inorganic and Coordination Compounds,* 4th ed.; John Wiley & Sons: New York, 1986.
(22) Payen, E.; Grimblot, J.; Lavalley, J. C.; Daturi, M.; Maugé, F. Application of Vibrational Spectroscopy in the Study of Oxide (Excluding Zeolites) and Sulfide Catalysts, in Industry, Materials and

the Physical Sciences. In *Handbook of Vibrational Spectroscopy*; Chalmers, J. M., Griffith, P. R., Eds.; Wiley: New York, 2006; Vol. 4.
(23) Kumada, N.; Takahashi, M.; Kinomura, N.; Sleight, A. W. *J. Solid State Chem.* **1996**, *126*, 121.
(24) Kumada, N.; Takahashi, M.; Kinomura, N.; Sleight, A. W. *Mater. Res. Bull.* **1997**, *32*, 1003.
(25) Negas, T.; Roth, R. S. *J. Solid State Chem.* **1971**, *3*, 323.
(26) Shpanchenko, R. V.; Nistor, L.; Van Tendeloo, G.; van Landuyt, J.; Amelinckx, S.; Abakumov, A. M.; Antipov, E. V.; Kovba, L. M. *J. Solid State Chem.* **1995**, *114*, 560.
(27) Blake, G. R.; Battle, P. D.; Sloan, J.; Vente, J. F.; Darriet, J.; Weill, F. *Chem. Mater.* **1999**, *11*, 1551.
(28) Shpanchenko, R. V.; Abakumov, A. M.; Antipov, E. V.; Kovba, L. M. *J. Alloys Compd.* **1994**, *206*, 185.
(29) Hong, S. T.; Sleight, A. W. *J. Solid State Chem.* **1997**, *132*, 407.
(30) Darriet, J.; Subramanian, M. A. *J. Mater. Chem.* **1995**, *5*, 543.
(31) Blake, G. R.; Sloan, J.; Vente, J. F.; Battle, P. D. *Chem. Mater.* **1998**, *10*, 3536.
(32) Wilkens, J.; Müller-Buschbaum, Hk. *J. Less-Common Met.* **1991**, *171*, 255.
(33) Dijskma, F. J. J.; Vente, J. F.; Frikkee, E.; Ijdo, D. J. W. *Mater. Res. Bull.* **1993**, *28*, 1145.
(34) Quarez, E.; Huvé, M.; Abraham, F.; Mentré, O. *Solid State Sci.* **2003**, *5*, 951.
(35) Boulahya, K.; Amador, U.; Parras, M.; Gonzalez-Calbet, J. M. *Chem. Mater.* **2000**, *12*, 966.